International Journal of Electrical Engineering & Emerging Technology, Vol. 07, No. 01, JUN 2024, pp 01-07

BOOST INVERTER USING SLIDING MODE CONTROLLER FOR PHOTOVOLTAIC APPLICATIONS

Nirmal Samejo [a]
[a]Department of Electrical Engineering, Mehran University of Engineering & Technology, Jamshoro, 76062, Pakistan
Corresponding author e-mail: (nirmalsamejo98@gmail.com)
[**Received on:** 01-04-2024 **Accepted on**: 09-05-2024 **Published on:** 24-06-2024]

***Abstract*: This research paper presents an enhanced power conversion strategy for photovoltaic systems through the application of a sliding mode controller for a boost inverter circuit comprising of four IGBT switches. The proposed system seeks to capitalize on the inherent advantages of boost inverters, such as high power density and efficiency, while addressing the dynamic challenges posed by PV systems. The integration of the SMC aims to harness its robustness against system uncertainties and external disturbances, ensuring optimal performance in power conversion. In a comparative evaluation, the conventional PID controller was also implemented for benchmarking purposes. Through rigorous simulation studies, it was determined that the SMC consistently outperformed the PID controller, offering superior regulation, faster transient response, and lower output voltage distortion in the face of varying solar irradiances and load conditions. The simulation results validate the potential of the SMC-equipped boost inverter, marking a substantial improvement over traditional PID-based systems in terms of reliability and efficiency for photovoltaic applications. This investigation underscores the efficacy of sliding mode control as a promising alternative for advancing the state of PV energy conversion systems.**

***Index Terms*— Boost Inverter, Converter, PID, PV, SMC.**

I. INTRODUCTION

PV systems have revolutionized the production of clean and uninterrupted power. However, PV cell output voltage is not constant and is highly dependent on temperature, load current, and irradiance. This is where converters play a crucial role in ensuring a consistent voltage output from the PV system [1]. The boost inverter, also known as the boost DC-AC converter, has a unique characteristic. It can produce an output AC voltage that is greater than the input DC voltage, by varying the duty cycle. It differs from a conventional voltage source inverter in that it produces an AC output voltage that is constantly lower than the DC input voltage [2]. The operation of the converters can be managed using a range of control techniques and algorithms. Various control approaches like PI, PID, SMC, and control system are employed to regulate the performance and voltage of the converter[3-5].

This work proposes a boost inverter and uses two control strategies to adjust the inverter voltage. Both controllers are analyzed to find which one performs better.

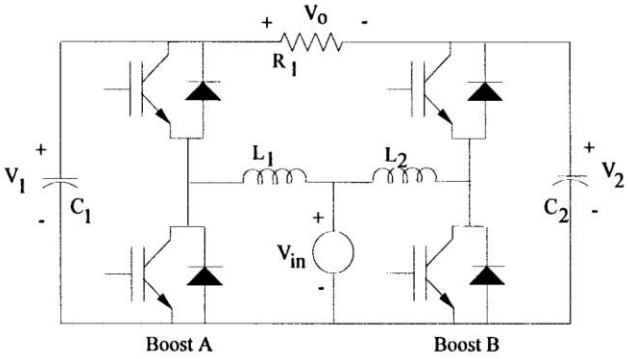

Fig. 1. Boost Inverter

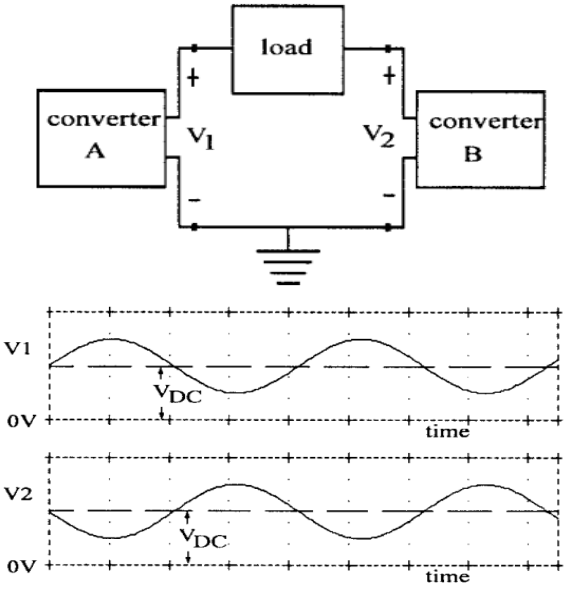

Fig. 2. A fundamental method for achieving boost characteristics in dc–ac conversion.

To produce a dc-ac conversion, the proposed boost inverter connects the two dc-dc converters' loads differently and sinusoidally regulates the output voltages of the converters as shown in the Fig. 2 [6]. DC-DC converters are represented by blocks A and B. Each source only generates a unipolar voltage

using each of these converters, which provide an output that is a dc-biased sine wave. The fluctuation of voltage over the load is maximized by each converter's 180-degree out of phase modulation. Differentially connected across the converters is the load.

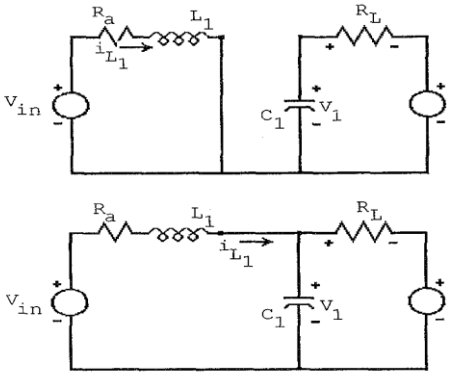

Fig. 3. Modes of Operation

Voltage V_1 decreases when switch S_1 is closed and switch S_2 is open (Fig. 3), causing current i_{Ll} to climb fairly linearly, diode D_2 to be reverse biased, and capacitor C_1 to supply energy to the output stage. Following the flip of switches S_1 and S_2 (Fig. 3). Current passes through the output stage and capacitor C1. During the recharge of capacitor C1, the current iL1 decreases. The state variables i_{Ll} and V_l with equivalent circuit of the state space modelling, gives:

$$\begin{bmatrix} \frac{di_L}{dt} \\ \frac{dV_1}{dt} \end{bmatrix} = \begin{bmatrix} \frac{-Ra}{L1} & \frac{-1}{L1} \\ \frac{1}{L1} & \frac{-1}{L1} \end{bmatrix} \begin{bmatrix} i_L \\ V_1 \end{bmatrix} + \begin{bmatrix} \frac{V_1}{L} \\ -\frac{i_L}{C} \end{bmatrix} \gamma + \begin{bmatrix} \frac{V_{in}}{L1} \\ \frac{V_2}{C1\mathrm{RL}} \end{bmatrix}$$

$$V = Av + B\gamma + C \qquad (1)$$

where V and **v** are the vectors of the status variables (i_{L1}, V_1) and their time derivatives respectively. As **γ** is the switches status.

$$\gamma = \begin{Bmatrix} 1, when\ S1\ ON,\ \ S2\ OFF \\ 0, when\ S1\ OFF,\ \ S2\ ON \end{Bmatrix} \qquad (2)$$

II. Sliding Mode Controller

Control of switching power converters has been compared effectively with sliding mode control. The primary benefit of traditional control techniques is intrinsic resistance to changes in plant parameters, which, in the ideal condition, results in steady-state effect and invariant dynamics. A boost inverter's sliding mode controller is suggested in this research. The fundamental principle behind SMC is that, once the system reaches the SM, it is naturally restricted to a certain range and is impervious to parametric fluctuations and disturbances. The sliding surface must be defined in order to meet the requirements for convergence to the system's solution or to the sliding regime[7]. When an output voltage's good transient response is required, a sliding surface S(iLl, Vl) might be selected to be [2]

$$S(i_{Ll}, V_l) = K1\varepsilon_1 + K2\varepsilon_2 = 0 \qquad (3)$$

A linear combination of state variable errors ε1 expresses the sliding surface equation $S(i_{Ll},V_l)$ in the state space. In this case, the feedback voltage error is denoted by ε_2, and the feedback current error by ε_1.

$$\varepsilon_1 = i_L - i_{Lref} \qquad (4)$$

$$\varepsilon_2 = V1 - V_{ref} \qquad (5)$$

Substituting (4) and (5) in (3), it is obtained:

$$S(iL1, V1) = K(i_L - i_{Lref}) + (V1 - V_{ref}) \qquad (6)$$

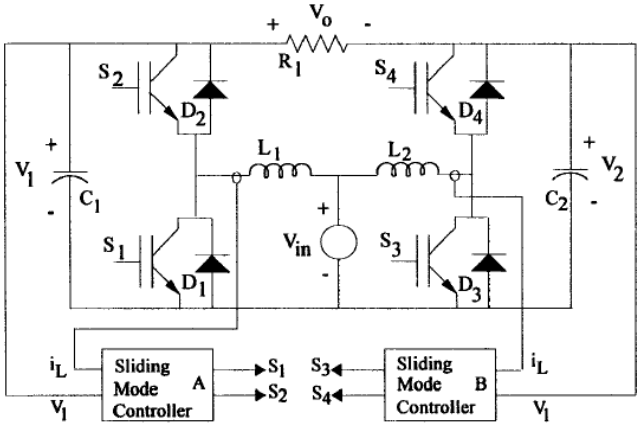

Fig. 4. The sliding mode controls the boost inverter.

By using the hardware implementation of equation (9) to create the signal $S(i_{L1},V1)$, a basic circuit known as a hysteresis comparator may provide the pulses required to power semiconductor drives. Fig. 5 displays the same control scheme. Hysteresis block H1 regulates the status of the switch γ by keeping the variable $S(i_{L1},V_1)$ close to zero. The coefficients K1 and K2, as well as the circuit characteristics, affect the system response. High control robustness, stability, and quick response can be attained with the right use of these coefficients under any operating situation. According to theory, in order to regulate the sliding mode, all state variables must be sensed and appropriate references must be created for each one. Since the inductor current reference typically varies on the supply voltage, load voltage, and load power demand, it is challenging to evaluate. In order to solve this issue, If the low-frequency component of the high-pass filter is automatically adjusted to the actual converter operation, the state variable error for the inductor current ($i_{L1} - i_{Lref}$) can be extracted from the feedback variable i_{L1}. As a result, the control just needs this

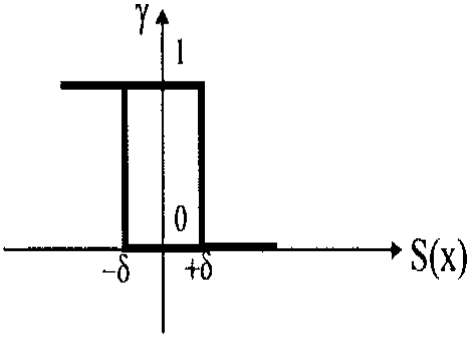

Fig.5 Switching Function

variable's high-frequency component. The converter dynamics can be considerably altered by this high-pass filter, which also increases the system's order. The high-pass filter's cutoff frequency needs to be sufficiently lower than the switching frequency in order to pass the ripple at the switching frequency and prevent this issue, high enough to enable quick response from the converter [8]. Coefficients K_1 and K_2 define the behavior of the system entirely and must be chosen to guarantee stability, quick response times, and existence even in the face of significant variations in supply and load. According to the variable structure system theory, the converter equations must be written as follows:

$$\dot{x} = Ax + B\gamma + D \tag{7}$$

where x is the state-variable errors vector, as indicated by

$$x = v - V^* \tag{8}$$

where $V^* = [i_{Lref}, V_{ref}]^T$ is the vector of references (index **T** denotes transposition).
Substituting (8) in (1) it is obtained:

$$D = AV^* + C \tag{9}$$

$$D = \begin{bmatrix} \frac{-Ra}{L1} & \frac{-1}{L1} \\ \frac{1}{L1} & \frac{-1}{L1} \end{bmatrix} \begin{bmatrix} i_L \\ V_1 \end{bmatrix} + \begin{bmatrix} \frac{V_{in}}{L1} \\ \frac{V_2}{C1RL} \end{bmatrix}$$

$$\mathbf{D} = \begin{bmatrix} -\frac{\mathbf{V_{ref}}}{\mathbf{L_1}} + \frac{\mathbf{V_{in}}}{\mathbf{L_1}} - \frac{\mathbf{R_a i_{Lref}}}{\mathbf{L_1}} \\ -\frac{\mathbf{V_{ref}}}{\mathbf{C_1 R_L}} + \frac{\mathbf{V_2}}{\mathbf{C_1 R_L}} + \frac{\mathbf{i_{Lref}}}{\mathbf{C_1}} \end{bmatrix} \tag{10}$$

Substituting (8) in (6), the sliding function can be rewritten in the form:

$$S(x) = kx_1 + k_2x_2 = k^Tx = 0 \tag{11}$$

All state trajectories close to the surface must point in the direction of the sliding plane in order for the sliding mode to exist. By using the converter switches correctly, the controller may make the system stay close to the sliding plane. All state trajectories close to the surface must point in the direction of the sliding plane in order for the sliding mode to exist. The system state can be forced by the controller to stay close to the sliding plane through appropriate the converter switches' functionality.

$$\left.\begin{matrix} \dot{S} < 0 \ \ if \ \ S > 0 \\ \dot{S} > 0 \ \ if \ \ S < 0 \end{matrix}\right\} \tag{12}$$

It is required and sufficient that in order for the system state to flow in the direction of the switching surface. The subsequent feedback control method results in sliding mode control by linking the switches state to the value of S(x).

$$\gamma = \left\{\begin{matrix} 0\,, when\ S(x) > 0 \\ 1, when\ S(x) < 1 \end{matrix}\right\} \tag{13}$$

The following is an expression for the existence condition (12):

$$\dot{S}(x) = K^TAx + K^TD < 0; \ \ 0 < S(x) < \delta \tag{14}$$

$$\dot{S}(x) = K^TAx + K^TB + K^TD > 0; \ -\delta < S(x) < 0 \tag{15}$$

where δ is a positive quantity that can have any size.
Assuming, from a practical perspective, that error variables X_1 are appropriately smaller than references V*,
It is possible to rewrite (14) and (15) as follows:

$$K^TD < 0\,; \qquad 0 < S(x) < \delta \tag{16}$$

$$K^TB + K^TD > 0; \ \ -\delta < S(x) < 0 \tag{17}$$

Substituting matrices B and D in (16) and (17), it is obtained:

$$\frac{\mathbf{K_1}}{\mathbf{L_1}}\left[\mathbf{V_{in} - V_{ref} - R_a i_{Lref}}\right] + \frac{\mathbf{K_2}}{\mathbf{C_1 R_L}}\left[\mathbf{V_2 - V_{ref} + R_L i_{Lref}}\right] < 0 \tag{18}$$

$$\frac{\mathbf{K_1}}{\mathbf{L_1}}\left[\mathbf{V_{in} - R_a i_{Lref}}\right] + \frac{\mathbf{K_2}}{\mathbf{C_1 R_L}}\left[\mathbf{V_2 - V_{ref}}\right] > 0 \tag{19}$$

The existence condition is satisfied if the inequalities (18) and (19) are true.

Finally, it's important to ensure that all initial states reach the intended sliding plane. In the system represented by (7), K1 and K2, which are non-negative coefficients, are necessary for the sliding mode to exist. The circuit parameters and coefficients K_1 and K_2 must be determined in order to attain the desired values for maximum inductor current ripple, maximum capacitor voltage ripple, maximum switching frequency, stability, and fast response under all operating situations.

III. Proportional, Derivative, Integral Controller

Among industrial control applications, proportional-integrative-derivative (PID) controllers are without a doubt the most comprehensive choice [9]. Due to the difficulty of tuning, approximately 75% of PID applications worldwide are still not properly calibrated. It is necessary to systematically include the uncertainties in the design process in addition to the intended closed-loop performance standards[10]. A simple feedback system is illustrated by the block diagram in Fig. 6.

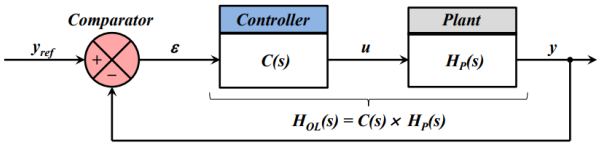

Fig. 6. Block Diagram of Feedback Control

The controller was developed to fulfill the three primary criteria for feedback control: stability, a damping ratio around unity, accuracy (particularly in steady states), and step response settling time (within a 5% error band). [EEEPE 40002] The following represents the closed-loop transfer function $H\mathrm{CL}(s)$:

$$H_{CL}(s) = \frac{Y(s)}{Y_{ref}(s)} = \frac{H_{OL}(s)}{1 + H_{OL}(s)} \tag{20}$$

Hence, it derives that:

$$\begin{aligned} |H_{OL}(j\omega)| \gg 1 \quad &\rightarrow \quad H_{CL}(j\omega) \cong \frac{H_{OL}(j\omega)}{H_{OL}(j\omega)} = 1 \\ |H_{OL}(j\omega)| \ll 1 \quad &\rightarrow \quad H_{CL}(j\omega) \cong \frac{H_{OL}(j\omega)}{1} = H_{OL}(j\omega) \end{aligned} \tag{21}$$

High open-loop gain $|HO\mathrm{L}(\mathrm{j}\omega)|$ above the LF boundary at low frequency (LF) indicates a closed-loop gain value around unity, which results in high steady state accuracy and effective tracking of the LF reference signal even when model uncertainties are taken into account.
The time-domain equation of the PID controller is:

$$u(t) = K_P\left(\varepsilon(t) + \frac{1}{T_I}\int_0^t \varepsilon(\tau).d\tau + T_D\frac{d\varepsilon}{dt}(t)\right) \tag{22}$$

which, in Laplace transform, is:

$$C_{PID}(s) = \frac{U(s)}{\varepsilon(s)} = K_P\left(1 + \frac{1}{T_I s} + T_D s\right) = K_P\left(\frac{1 + T_I s + T_I T_D s^2}{T_I s}\right) \tag{23}$$

Three independent additional terms are combined in the PID transfer function:

1. The proportional term (KP), which applies at any frequency and allows the cross frequency (ω_X) and, in turn, the settling time ($t_{S\mathrm{T,5\%}}$ to be adjusted).
2. The integral term (K_P/T_{1s}), which mostly functions at low frequency ($\omega < 1/T_I$), offers an appealing rejection of model uncertainties along with a high gain and, thus, an accurate LF. Additionally, this term causes a 90° phase delay that could be unstable.
3. Large three phase and gain margins are paired with a stabilizing 90° phase lead provided by the derivative term ($K_P T_{DS}$), which functions mostly at high frequency $\omega > 1/T_D$ [11].

The plant enters an open-loop state when the control value crosses a threshold, and the integrator continues to integrate, progressively producing a large value. Large overshoots and potentially unstable responses are the consequence[12]

IV. Simulation Results

The simulation is conducted using MATLAB/Simulink, as shown in Fig. 7 considering a constant power supply voltage, optimal power switches, and optimal output capacitors. The simulation employs the parameters shown in Table 1 to accurately reflect the system's behavior.

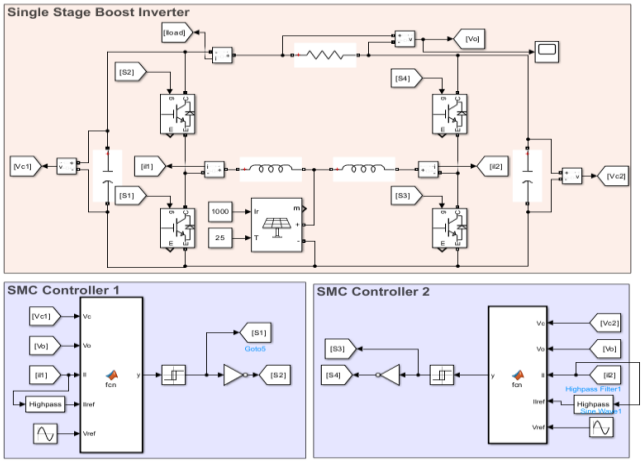

Fig. 7. Proposed Boost inverter scheme with SMC

TABLE I: Boost Inverter using SMC parameters [2].

Component	Value
Inductor	800 µH
Capacitor	40 µF
Switching frequency	60 Hz
Input Voltage	90 V
Specification of Panel:	25°C, 1000 W/m^2
Coefficients KI, K2	0.208, 0.040

Controller produces sinusoidal waveform on both of capacitors C_1 and C_2 as seen in Fig. 8, the difference between those is applied to the load resulting in a 110 Vrms sinusoidal voltage across load.

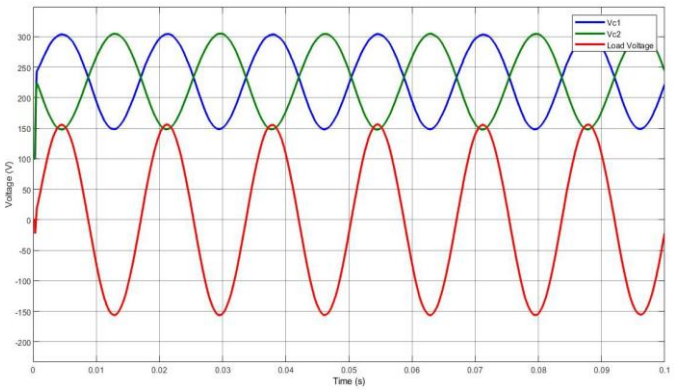

Fig. 8. Capacitors C_1, C_2 and load voltage

The load voltage and current waveform is illustrated in Fig. 9, the input DC voltage is shown in a red line at 90 V which is lower than the peak AC voltage at load.

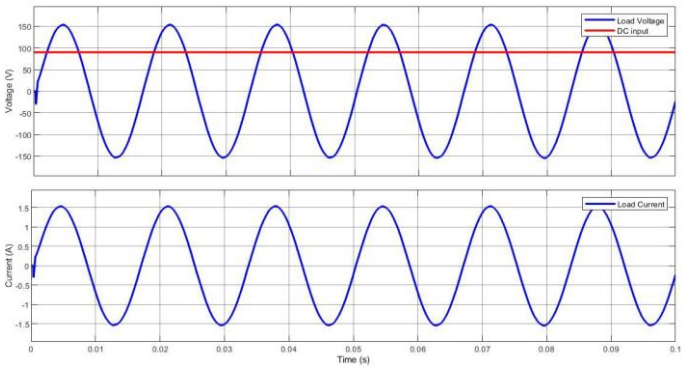

Fig. 9. Load voltage and current at 90 VDC input

The harmonic analysis of the output shows that the total harmonic distortion is at 0.69% which is well under acceptable range of 5% set by IEEE 519 standard.

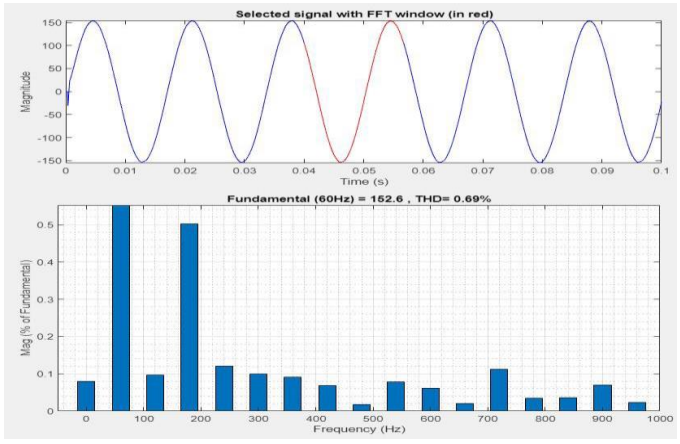

Fig. 9. THD analysis of output waveform

To show the effect of voltage variation, the voltage of input was increased from 90 V to 130 V. The output remained stable and sinusoidal even at 44% of voltage variation at shown in Fig. 11.

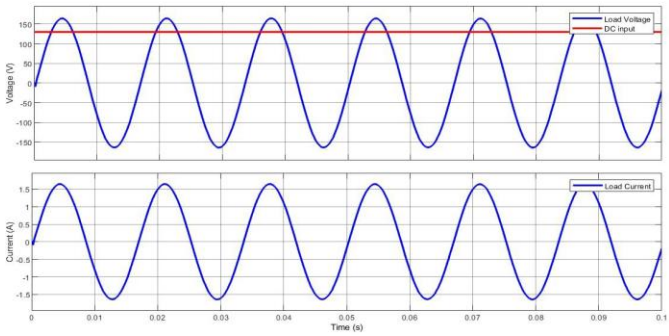

Fig. 11. Load voltage and current at 130 VDC input

The harmonic analysis at 130 VDC shows even lower harmonic distortion this time of 0.44%, this decrease is attributed to lower boosting required as the input voltage is higher than before.

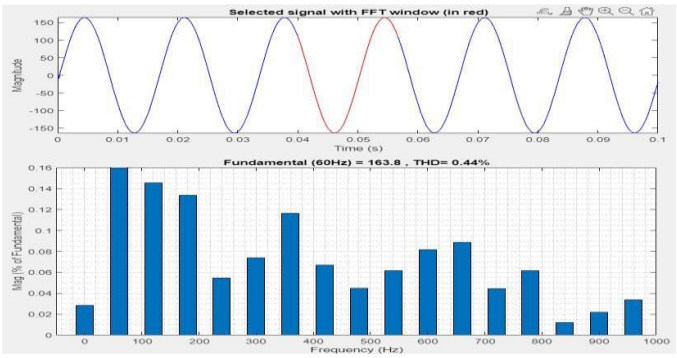

Fig. 12. THD analysis of output waveform at 130 VDC

V. Comparison with Conventional PID Controller

To validate the performance of SMC, it is compared to conventional PID Controller, the controller is designed in Simulink, the model is given in Fig. 13.

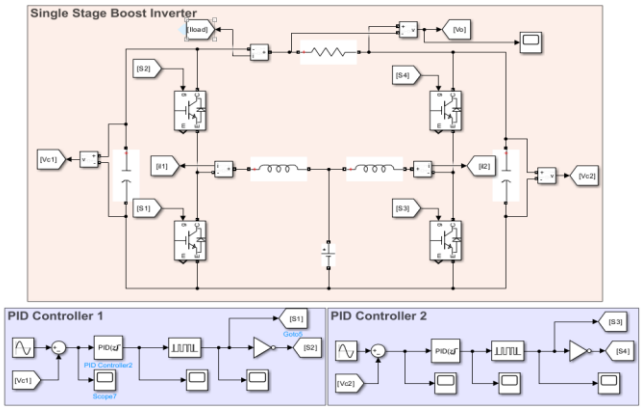

Fig. 13. Proposed Boost inverter using PID

The output waveform of capacitor voltages in Fig. 14 show some level of distortion and oscillations at the beginning of the startup, issues that was not seen in SMC controlled boost inverter.

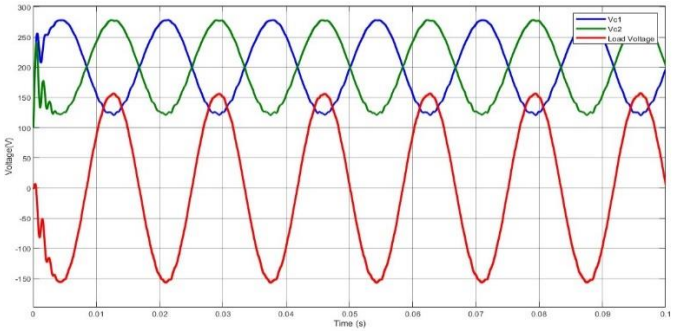

Fig. 14. Capacitors C1, C2 and load voltage with PID

The load voltage and current waveform is illustrated in Fig.15 the input DC voltage is shown in a red line at 90 V which is lower than the peak AC voltage at load. Waveforms are sinusoidal except the oscillations at start.

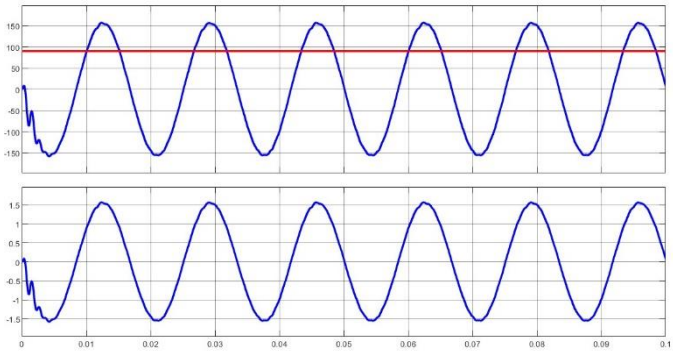

Fig. 15. Load voltage and current at 90 VDC input with PID

The harmonic analysis of PID controlled inverter shows THD of 1.08%, on the other hand, the THD was 0.69% for SMC controlled inverter

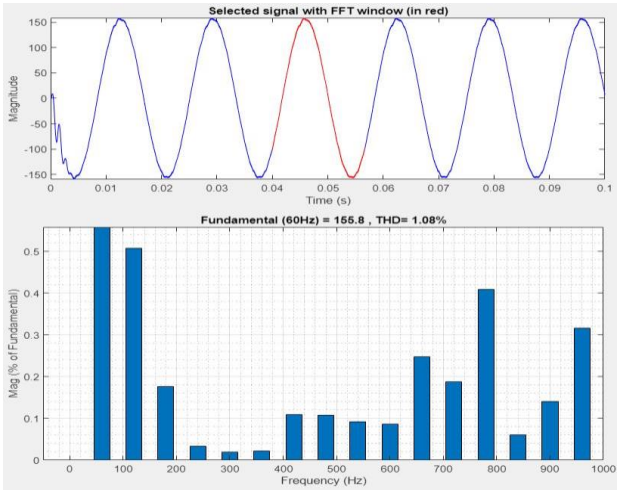

Fig. 16. THD analysis of output waveform with PID

In a similar fashion of voltage variation in SMC case, the voltage was increase to 130 V for PID controller and significant distortion was seen in waveforms.

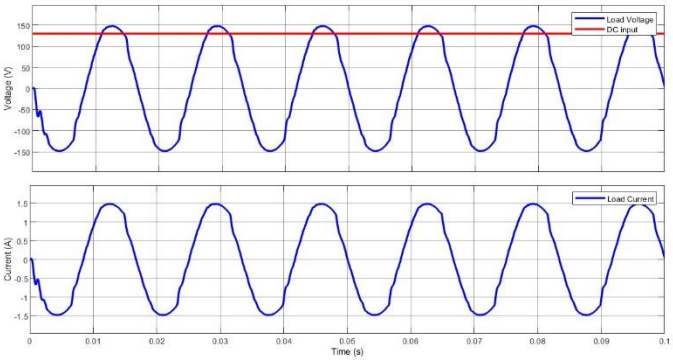

Fig. 17. Load voltage and current at 130 VDC input with PID

Due to distortion, the THD increased to above 5% acceptable limits as shown in Fig. 18.

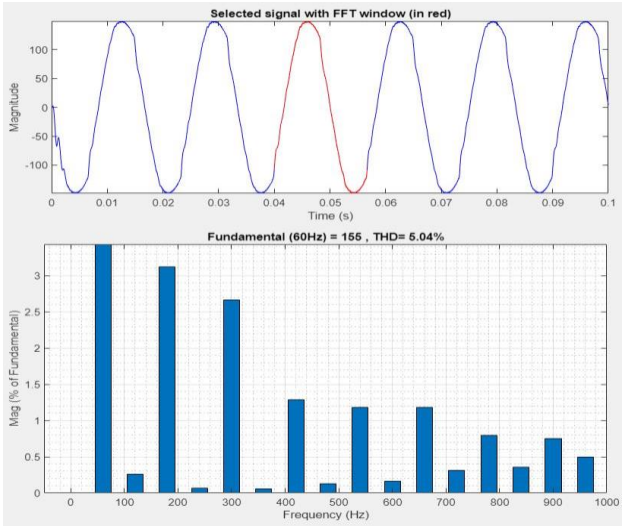

Fig. 18. THD analysis of output at 130 VDC with PID

The plant enters an open-loop state when the control value crosses a threshold, and the integrator continues to integrate, progressively producing a large value. Large overshoots and potentially unstable responses are the consequence.

VI. CONCLUSION

In conclusion, the experimental analysis conducted on the four-IGBT switch boost inverter integrated with a photovoltaic system demonstrates the strategic advantages of deploying a sliding mode controller over a conventional PID controller. The boost inverter, a critical component designed to step up the output voltage to desired levels, was subjected to rigorous testing under various conditions. While the PID controller showed vulnerabilities, leading to disturbances in the output waveform, the SMC maintained a robust and consistent performance even with 44% of input voltage change, free from such perturbations. Notably, the SMC proved its mettle by producing a stable output voltage waveform even amidst voltage and load variations, showcasing its exceptional

capability in disturbance rejection. Error was found to be 0.1V for SMC and 0.4V for PID, which are both good results, however with SMC being slightly better. The harmonic analysis of PID controlled inverter shows THD of 1.08%, on the other hand, the THD was 0.69% for SMC controlled inverter. These findings underscore the sliding mode controller's potential in optimizing boost inverter functionality, which is essential for the effective utilization of photovoltaic systems. The simulation results validate the potential of the SMC-equipped boost inverter, marking a substantial improvement over traditional PID-based systems in terms of reliability and efficiency for photovoltaic applications. Thus, the research confirms that the SMC is the preferable choice for controlling boost inverters in environments that demand high reliability and stability against internal and external fluctuations.

VII. REFERENCES

1. Mohanty, S., et al. *A comparative analysis between a single loop PI, double loop PI and Sliding Mode Control structure for a buck converter*. in *2021 1st Odisha International Conference on Electrical Power Engineering, Communication and Computing Technology (ODICON)*. 2021. IEEE.
2. Caceres, R.O. and I. Barbi, *A boost DC-AC converter: analysis, design, and experimentation.* IEEE transactions on power electronics, 1999. **14**(1): p. 134-141.
3. Kalimuthukumar, S., et al. *A sliding mode controller based boost converter for grid connected solar PV system*. in *2021 international conference on advance computing and innovative technologies in engineering (ICACITE)*. 2021. IEEE.
4. Li, X., et al., *An improved MPPT method for PV system with fast-converging speed and zero oscillation*. IEEE Transactions on Industry Applications, 2016. **52**(6): p. 5051-5064.
5. Varma, R.K. and R. Salehi, *SSR mitigation with a new control of PV solar farm as STATCOM (PV-STATCOM).* IEEE Transactions on Sustainable Energy, 2017. **8**(4): p. 1473-1483.
6. Carpita, M., P. Farina, and S. Tenconi. *A single phase, Sliding Mode Controlled Inverter with three levels output voltage for UPS or Power Conditioning Applications*. in *1993 Fifth European Conference on Power Electronics and Applications*. 1993. IET.
7. Inomoto, R.S., J.R.B. de Almeida Monteiro, and A.J. Sguarezi Filho, *Boost converter control of PV system using sliding mode control with integrative sliding surface.* IEEE Journal of Emerging and Selected Topics in Power Electronics, 2022. **10**(5): p. 5522-5530.
8. Mattavelli, P., et al. *General-purpose sliding-mode controller for DC/DC converter applications*. in *Proceedings of IEEE Power Electronics Specialist Conference-PESC'93*. 1993. IEEE.
9. Åström, K.J. and T. Hägglund, *The future of PID control.* Control engineering practice, 2001. **9**(11): p. 1163-1175.
10. Kobaku, T., R. Poola, and V. Agarwal, *Design of robust PID controller using PSO-based automated QFT for nonminimum phase boost converter.* IEEE Transactions on Circuits and Systems II: Express Briefs, 2022. **69**(12): p. 4854-4858.
11. Béthoux, O., *Linear Controllers: PID controller design*. Reference Module in Materials Science and Materials Engineering, 2022.
12. da Silva, L.R., R.C. Flesch, and J.E. Normey-Rico, *Analysis of anti-windup techniques in PID control of processes with measurement noise.* IFAC-PapersOnLine, 2018. **51**(4): p. 948-953.